Direct Dynamics Study of the Dissociation and Elimination Channels in the Thermal Decomposition of Methyl Nitrite

Antonio Fernández-Ramos,† Emilio Martínez-Núñez,† Miguel A. Ríos,† Jesús Rodríguez-Otero,† Saulo A. Vázquez,*,† and Carlos M. Estévez‡

Contribution from the Departamento de Química Física, Universidad de Santiago de Compostela, 15706 Santiago de Compostela, Galicia, Spain, and Departamento de Química Física y Química Orgánica, Facultad de Ciencias de Vigo, Universidad de Vigo, Vigo, Galicia, Spain

Received March 19, 1998. Revised Manuscript Received May 18, 1998

Abstract: The dynamics of the two unimolecular reactions that initiate the thermal decomposition of methyl nitrite were investigated by direct dynamics calculations. The two decomposition pathways are (I) O−N bond scission to form CH_3O and NO and (II) concerted elimination through a four-center transition state to produce CH_2O and HNO. Structural data along the reaction paths were obtained from high-level ab initio methods. Specifically, the elimination reaction path was achieved from MP2 results scaled so that the height of the barrier coincided with the value given by QCISD(T)//QCISD calculations. The dissociation path was first calculated at the CASSCF(8,8) level of theory and then scaled to reproduce the dissociation energy predicted by QCISD(T)//CASSCF(8,8) computations. All the ab initio calculations were performed with the standard 6-311++G(d,p) basis set. Thermal rate constants were evaluated by canonical variational transition-state theory (CVT). For the elimination process, tunneling was taken into account by using the approximations zero curvature tunneling (ZCT) and small curvature tunneling (SCT). The overall agreement between the calculated rate constants and the experimental ones reported in the literature is reasonably good. The calculations indicate that the dissociation is remarkably faster than the elimination not only because the barrier height for the O−N bond scission is lower than that for the elimination reaction but also because the former process is entropically favored.

1. Introduction

The pyrolysis and photolysis of methyl nitrite (MeONO) has been the focus of many investigations because it is a convenient source of the methoxy radical, which is very important to combustion and atmospheric chemistry. Early work on the pyrolysis of MeONO by Steacie and Shaw[1] suggested that the cleavage of the CH_3O-NO bond was the first step in the thermal decomposition process. A second reaction then converted CH_3O to CH_3OH and CH_2O. Subsequent experimental studies,[2−8] however, pointed out that the actual mechanism is much more involved. In particular, He et al.[8] proposed a mechanism including as many as 16 elementary steps, with six of them being considered as key reactions. Their detailed kinetic modeling, aided by Rice−Ramsperger−Kassel−Marcus (RRKM) calculations, afforded a quantitative description of the disappearance of methyl nitrite and the formation of all major products.

According to the accumulated experimental data, the overall thermal decomposition of MeONO is basically initiated by the aforementioned dissociation process:

$$CH_3ONO \rightarrow CH_3O + NO \qquad (I)$$

Most of the proposed mechanisms also include one more unimolecular decomposition channel that is believed to proceed through a four-center transition state:

$$CH_3ONO \rightarrow CH_2O + HNO \qquad (II)$$

The O−N bond scission is markedly faster than the intramolecular elimination reaction. The ratio k_I/k_{II} estimated experimentally by Batt et al.[6] in the temperature range 443−447 K is 10, and that computed from the rate constants reported by He et al.[8] is even greater.

In this paper, rate constants for the two competing channels that initiate the thermal decomposition of MeONO (reactions I and II) are evaluated by direct dynamics calculations; that is, the dynamics calculations are based directly on the electronic structure data without the intermediary of a fit. We begin with an ab initio investigation carried out at high levels of theory so as to obtain accurate data (energetics, frequencies, and reaction paths) on these two reaction channels. Then we apply canonical variational transition-state theory (CVT) with semiclassical corrections for tunneling to compute thermal rate constants at temperatures in the range 300−1500 K.

2. Methodology

2.1. Ab Initio Calculations. The geometries of the stationary points involved in the elimination reaction (reactant,

* Corresponding author. Fax: 34-81-595012.
† Universidad de Santiago de Compostela.
‡ Universidad de Vigo.

(1) Steacie, E. W. P.; Show, G. T. *Proc. R. Soc., Ser. A* **1934**, *A146*, 388.
(2) Carter, A. G.; Travers, M. W. *Proc. R. Soc., Ser. A* **1937**, *A158*, 495.
(3) Gray, P.; Williams, A. *Nature (London)* **1960**, *56,* 188.
(4) Phillips, L *J. Chem. Soc.* **1961**, *7*, 3082.
(5) Zaslonko, I. S.; Kogarko, S. M.; Mozzhukhin, E. V.; Petrov, Yu. P.; Borisov, A. A. *Kinet. Katal*. **1970**, 11, 296.
(6) Batt, L.; Milne, R. T.; McCulloch, R. D. *Int. J. Chem. Kinet.* **1977**, *9*, 567.
(7) Hsu, D. S. Y.; Burkes, G. C.; Beebe, M. D.and Lin, M. C. *Int. J. Chem. Kinet.* **1984**, *16*, 1139.
(8) He, Y.; Sanders, W. A.; Lin, M. C. *J. Phys. Chem.* **1988**, *92*, 5474.

S0002-7863(98)00930-5 CCC: $15.00
Published on Web 07/15/1998

products, and a four-center transition state) were initially fully optimized with the GAUSSIAN94 package program[9] using the standard 6-311++G(d,p) basis set and the second-order Møller−Plesset perturbation theory (MP2)[10] to account for electronic correlation energy. Then quadratic CI full optimizations including single and double substitutions (QCISD),[11] as well as single-point QCISD(T) (a triples contribution to the energy is added) calculations at the QCISD-optimized geometries were also carried out, employing the above basis set, so as to improve the energetic predictions. Normal-mode analyses were performed to verify that the minima have all positive frequencies and that the transition state has only one imaginary frequency with the corresponding eigenvector pointing toward the reactant or the product. The harmonic vibrational frequencies were obtained by diagonalizing the mass-weighted Cartesian force constant matrix, calculated from analytical second derivatives of the total energy at the MP2 level of theory.

Starting from the saddle-point geometry we have constructed the minimum energy path (MEP)[12,13] for the elimination reaction following the Gonzalez−Schlegel mass-weighted Cartesian-coordinates reaction path algorithm[14] at the MP2/6-311++G(d,p) level, with a stepsize of 0.01 a_0 amu$^{1/2}$ (a_0 = Bohr radius). Then, the MP2 potential was scaled to make the barrier height equal to the value given by the QCISD(T)//QCISD computations. For subsequent kinetic calculations, the matrices of force constants were evaluated at the MP2 level of theory every 0.1 a_0 amu$^{1/2}$ along the path. We found no significant changes in the calculated rate constants when the step size used for Hessian evaluations was reduced. All calculations were performed in the mass-scaled Cartesian coordinate system in which all mass-weighted Cartesian coordinates were scaled by $\mu^{-1/2}$, where μ is a single mass taken as the reduce mass of products (15.25 amu).

To study the dissociation surface we employed the CASSCF method,[15] which behaves properly at the dissociation limit, with an active space that comprised eight electrons in eight orbitals, and the 6-311++G(d,p) basis set.[16] A full geometry optimization was first carried out for the reactant (CH_3ONO). Then a series of partial optimizations was performed in which the O−N bond distance was gradually constrained from 1.7 to 3.5 Å by a step size of 0.3 Å, relaxing the remaining coordinates at each step. A final point at 10 Å was optimized, too, to ensure that we reached the dissociation products (CH_3O and NO) at about 3.5 Å. Second derivatives were calculated at each point by numerical differentiation. All CASSCF(8,8) calculations were done with the GAMESS 93 electronic structure code.[17] Single-point QCISD(T) calculations at the CASSCF-optimized geometries were also performed (with GAUSSIAN94) to improve the energetic results.

We used a distinguished-coordinate path (DCP)[18−20] instead of an MEP to define the reaction path and reaction coordinate in the dissociation channel because there is no saddle point. We found that the O−N bond distance was the most important varying parameter; consequently, we selected this geometrical feature as the distinguished coordinate. Thus, in this study, the DCP is defined as the sequence of minimum energy structures obtained for several fixed values of the O−N distance. Following the procedure employed in the elimination channel, we scaled the CASSCF potential to make the dissociation energy (D_e) equal to the value given by the QCISD(T)//CASSCF(8,8) calculations. In addition to the DCP thus determined, we have also utilized an improved DCP based on an algorithm developed recently by Villa and Truhlar[21] in which the orientation of the dividing surface is optimized. They called this reaction path the dynamically optimized DCP, and in this study, it will be referred to as the DODCP.

2.2. Kinetic Calculations. We applied canonical variational transition-state theory[23] to evaluate rate constants for the dissociation and elimination channels in the temperature range 300−1500 K. These calculations were undertaken with the POLYRATE package program (version 7.8.1).[22] In CVT, the rate constant, k^{CVT}, is defined as the least forward flux of trajectories through any family of curves perpendicular to the minimum energy path, for a given temperature T

$$k^{CVT}(T) = \min_s k^{GT}(T,s) \qquad (1)$$

where s is the reaction coordinate and $k^{GT}(T,s)$, the rate constant for passage through the generalized transition state (GTS) that intersects the MEP at s, is given by

$$k^{GT}(T,s) = \frac{\sigma k_B T}{h} \frac{Q^{GT}(T,s)}{Q_R(T)} \exp[-V_{MEP}(s)/(k_B T)] \qquad (2)$$

where σ is the symmetry factor, h and k_B are the Planck and Boltzmann constants, $V_{MEP}(s)$ is the potential energy of the MEP at s, and Q^R and Q^{GT} are the partition functions of the reactants and the GTS, respectively. The conventional transition-state rate constant, k^{TST}, corresponds to $s = 0$. The vibrational factors were calculated using the harmonic approximation, except for the torsional modes. For these modes we employed a formula derived previously by Truhlar[24] for hindered internal rotational modes, which gives reasonable accuracy over the whole range

(9) GAUSSIAN 94, Revision B.2: Frisch, M. J.; Trucks, G. W.; Schlegel, H. B.; Gill, P. M. W.; Johnson, B. G.; Robb, M. A.; Cheeseman, J. R.; Keith, T.; Petersson, G. A.; Montgomery, V.; Raghavachari, K.; Al-Laham, M. A.; Zakrzewski, V. G.; Ortiz, J. V.; Foresman, J. B.; Cioslowski, J.; Stefanov, B. B.; Nanayakkara, A.; Challacombe, M.; Peng, C. Y.; Ayala, P. Y.; Chen, W.; Wong, M. W.; Andres, J. L.; Replogle, E. S.; Gomperts, R.; Martin, R. L.; Fox, D. J.; Binkley, J. S.; Defrees, D. J.; Baker, J.; Stewart, J. P.; Head-Gordon, M.; Gonzalez, C.; Pople, J. A. Gaussian, Inc., Pittsburgh, PA, 1995.

(10) (a) Head-Gordon, M.; Pople, J. A.; Frisch, M. J. *Chem. Phys. Lett.* **1988**, *153*, 503. (b) Frisch, M. J.; Head-Gordon, M.; Pople, J. A. *Chem. Phys. Lett.* **1990**, *166*, 275. (c) Frisch, M. J.; Head-Gordon, M.; Pople, J. A. *Chem. Phys. Lett.* **1990**, *166*, 281.

(11) Pople, J. A.; Head-Gordon, M.; Raghavarachi, K. *J. Chem. Phys.* **1987**, *87*, 5968.

(12) Fukui, K. *Pure Appl. Chem.* **1992**, *54*, 1825.

(13) Truhlar, D. G.; Kuppermann, A. J. *J. Am. Chem. Soc.* **1971**, *93*, 1840.

(14) (a) González, C.; Schlegel, H. B. *J. Chem. Phys.* **1989**, *90*, 2154. (b) González, C.; Schlegel, H. B. *J. Phys. Chem.* **1990**, *94*, 5523.

(15) (a) Hegarty, D.; Robb, M. A. *Mol. Phys.* **1979**, *38*, 1795. (b) Eade, R. H. E.; Robb, M. A. *Chem Phys. Lett.* **1981**, *83*, 362.

(16) Due to limitations in the GAMESS 93 program we used Cartesian d functions.

(17) Schmidt, M. W.; Baldrige, K. K.; Boatz, J. A.; Elbertz, S. T.; Gordon, M. S.; Jensen, J. H.; Matsunaga, N.; Nguyen, K. A.; Su, S. J.; Windus, T. L., Dupuis, M.; Montgomery, J. A. *J. Comput. Chem.* **1993**, *14*, 1347.

(18) Rothman, M. J.; Lohr, L. L., Jr; Ewig, C. S.; van Wazer, J. R. *Potential energy surfaces and dynamics calculations*; Truhlar, D. G., Ed.; Plenum: New York, 1981; pp 653−660.

(19) Steckler, R.; Truhlar, D. G. *J. Chem. Phys.* **1990**, *93*, 6570.

(20) Heidrich, D. *The reaction path in chemistry*; Kluwer Academic Publishers: Dordrecht, The Netherlands, 1995; pp 1−10.

(21) Villà, J.; Truhlar, D. G. *Theor. Chem. Acc.* **1997**, *97*, 317.

(22) POLYRATE 7.8.1: Corchado, J. C.; Chuang, Y.-Y.; Fast, P. L.; Villá, J.; Coitiño, E. L.; Hu, W.-P.; Liu, Y.-P.; Lynch, G. C.; Nguyen, K. A.; Jackels, C. F.; Gu, M. Z.; Rossi, I.; Clayton, S.; Melissas, V. S.; Steckler, R.; Garret, B. C.; Isaacson, A. D.; Truhlar, D. G. University of Minnesota, Minneapolis, MN, 1998.

(23) Truhlar, D. G.; Issacson, A. D.; Garret, B. C. *Theory of Chemical Reaction Dynamics*; Baer, M., Ed.; CRC: Boca Raton, FL, 1985; Vol. 4, pp 65−137.

(24) Truhlar, D. G. *J. Comput. Chem.* **1991**, *12*, 266.

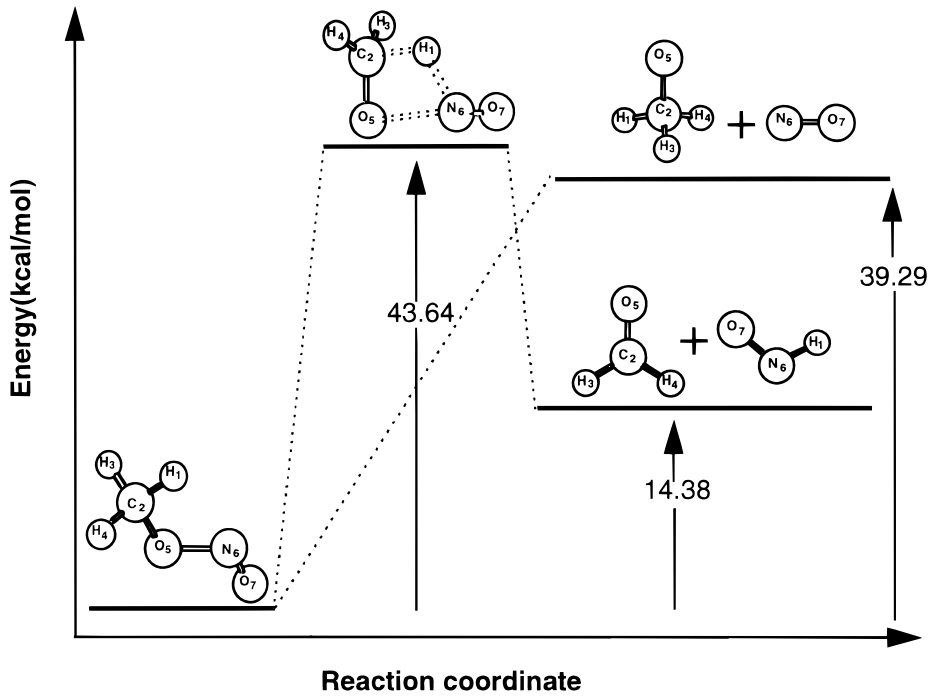

Figure 1. Energy diagram for the MeONO potential energy surface, showing reactant, saddle point, and asymptotic values of dissociation and elimination decomposition products.

from harmonic oscillator to hindered rotator to free rotator. For a unimolecular reaction the translational factors of the partition functions in eq 2 are equal and can therefore be ignored. In this study, we assumed that the contribution to the rate constant from the electronic partition functions is negligible.

Rate constants were corrected by means of transmission coefficients κ^{X} (where X indicates the approximation used):

$$k^{CVT/X}(T) = \kappa^{X} k^{CVT}(T) \tag{3}$$

where $k^{CVT/X}(T)$ is the corrected rate constant. For the dissociation process, we used the classical adiabatic ground-state (CAG) transmission coefficient,[25] $\kappa^{CVT/CAG}$, which corresponds to a classical correction for the reaction coordinate motion and allows one to estimate the microcanonical rate constant, $k^{\mu VT}(T)$. This coefficient is given by

$$\kappa^{CVT/CAG}(T) = \exp[-\beta\{V_a^G(s_*^{AG}) - V_a^G(s_*^{CVT})\}] \tag{4}$$

where s_*^{AG} is the value of the reaction coordinate at the top of the curve, s_*^{CVT} is the value of s minimizing $k^{GT}(T,s)$, and $V_a^G(s)$ is the vibrationally adiabatic ground-state curve, which is calculated as

$$V_a^G(s) = V_{MEP}(s) + \epsilon_{int}(s) \tag{5}$$

with $\epsilon_{int}(s)$ being the zero-point energy, at s, of vibrations that are orthogonal to the MEP. The s values were obtained from the set of DCP points computed as described in section 2.1, by fitting a curve through the DCP points.

For the elimination process, the classical transmission coefficient, $\kappa^{CVT/CAG}$, was calculated to be unity in the range of temperatures investigated. However, because in this case a light particle is transferred between two heavy atoms (*heavy*−*light*−*heavy* system), quantal effects such as tunneling should be considered. Accordingly, we have calculated the transmission coefficient by the expression

$$\kappa^{X} = \int_0^\infty P^{X}(E) e^{-\beta E}\, dE \Big/ \int_{V_a^G(s_*^{CVT})}^\infty e^{-\beta E}\, dE \tag{6}$$

where $\beta = 1/k_B T$ and $P^X(E)$ is the semiclassical transmission probability at total energy E in the approximation X. Specifically, we employed the approximations zero curvature tunneling (ZCT)[23,25] and small curvature tunneling (SCT).[23,26] In ZCT calculations, the curvature of the reaction path is assumed to be negligible, so that the tunneling path coincides with the MEP. In SCT calculations, which constitute a generalization of the Marcus−Coltrin method,[27] it is assumed that the tunneling path is displaced from the MEP to a concave-side vibrational turning point in the direction of the internal centrifugal force. This deviation is not explicitly calculated but is taken into account by calculation of a reduced mass, μ_{eff}, that is used in computing $P^{SCT}(E)$.

3. Results and Discussion

3.1. Minima and Elimination Transition State. It was postulated that the elimination reaction in both the thermal and the photolytic decompositions of methyl nitrite proceeds through a four-center transition state. For the photolytic decomposition of MeONO, Brown and Pimentel[28] had early suggested that CH_2O and HNO were formed by intramolecular elimination from the cis form of the nitrite. In this study, which concerns with the thermal decomposition, we located a transition state for the elimination reaction, which is a four-center arrangement with C_1 symmetry (see Figure 1). Additionally, we found that the elimination MEP connects this transition state with the products CH_2O and HNO as well as with the trans conformation of MeONO rather than the cis form. This prompted us to select

(25) Garret, B. C.; Truhlar, D. G.; Grev, R. S.; Magnuson, A. W. *J. Phys. Chem.* **1980**, *84*, 1730.
(26) Lu, D.-H.; Truong, T. N.; Melissas, V. S.; Lynch, G. C.; Liu, Y.-P.; Garret, B. C.; Steckler, R.; Issacson, A. D.; Rai, S. N.; Hancock, G. C.; Lauderdale, J. G.; Joseph, T.; Truhlar, D. G. *Comput. Phys. Commun.* **1992**, *71*, 235.
(27) Marcus, R. A.and Coltrin, M. E. *J. Chem. Phys.* **1977**, *67*, 2609.
(28) Brown, V.; Pimentel, G. C. *J. Chem Phys.* **1958**, *29*, 883.

Table 1. Equilibrium Geometries, Energetics, and Frequencies for the Chemical Species Involved in This Study[a]

internal coordinate	*trans*-CH_3ONO				transition state		$CH_2O + HNO$			$CH_3O + NO$	
	exptl[b]	MP2	CASSCF	QCISD	MP2	QCISD	exptl[c]	MP2	QCISD	exptl[d]	CASSCF
N_6O_7	1.164	1.182	1.189	1.175	1.157	1.138	1.212	1.221	1.207	1.15	1.154
O_5N_6	1.415	1.413	1.401	1.405	2.151	2.093					
C_2O_5	1.436	1.434	1.449	1.435	1.279	1.292	1.208	1.213	1.208	1.376	1.419
H_1C_2	1.09	1.091	1.079	1.091	1.423	1.331	1.116	1.105	1.107	1.094	1.086
H_3C_2	1.09	1.092	1.082	1.091	1.105	1.105	1.116	1.105	1.107	1.094	1.084
H_4C_2	1.09	1.092	1.082	1.091	1.105	1.104				1.094	1.084
H_1N_6					1.336	1.443	1.064	1.054	1.058		
$O_5N_6O_7$	111.8	111.3	109.7	111.0	119.3	118.8					
$C_2O_5N_6$	109.9	109.9	108.9	109.3	79.0	79.9					
$H_1C_2O_5$	109.5	109.5	104.7	105.3	99.9	102.1		122.0	122.0		
$H_3C_2O_5$	109.5	108.5	110.5	110.7	119.6	118.7		122.0	122.0		
$H_4C_2O_5$	109.5	108.5	110.5	110.7	119.6	118.7					
$H_1C_2H_3$		110.0		110.0	98.2	100.2	116.5	116.0	116.0	108.25	109.13
$H_1C_2H_4$		110.0		110.0	95.5	96.8				108.25	109.13
$H_3C_2H_4$		110.3		110.2	115.1	114.2				108.25	111.04
$H_1N_6O_7$					116.6	117.2	108.4	107.9	108.5		
$C_2O_5N_6O_7$		180.0	180.0	180.0	100.9	101.4					
$H_1C_2O_5N_6$		0.0	180.0	180.0	7.3	8.6					
$H_3C_2O_5N_6$		−120.1	61.0	60.4	112.6	117.4					
$H_4C_2O_5N_6$		120.1	−61.0	−60.4	−94.8	−96.3					
					Relative Energy						
	0.0	0.0	0.0	0.0	40.94	43.64[e]	15.3	15.14	14.38[e]	41.7	39.29[f]
					Harmonic Frequencies						
		78	107		1391i		1184	1207		717	729
	213	222	178		195		1282	1278		1064	1006
	379	379	373		254		1517	1559		1159	1123
	564	583	642		354		1779	1762		1582	1545
	812	834	906		541		2932	2974		1599	1563
	1031	1090	1083		730		2953	3045		1657	1620
	1043	1188	1230		1230					3216	3164
	1180	1220	1276		1238		1501	1499		3311	3235
	1424	1483	1564		1285		1565	1582		3320	3258
	1447	1501	1603		1420		2684	3033			
	1467	1534	1616		1495					1904	1872
	1665	1652	1665		1556						
	2822	3088	3196		1823						
	2882	3190	3274		2958						
	2912	3196	3307		3032						

[a] Distances given in angstroms, angles given in degrees, and energies given in kilocalories per mole. [b] Taken from refs 32, 35, and 36. [c] Taken from refs 37−42. [d] Taken from refs 43−46. [e] QCISD(T)/6-311++G(d,p)//QCISD/6-311++G(d,p) calculations. [f] QCISD(T)/6-311++G(d,p)//CASSCF/6-311++G(d,p) calculations.

the trans conformation as the reactant structure to be employed in the dynamical study. The trans form, however, is not the most stable conformation of MeONO, but its energy relative to the cis form, the most stable one, is less that 1 kcal/mol.[29−33] In particular, ab initio calculations performed at the QCISD/6-311++G(d,p) level of theory predict virtually the same energy for both conformations (the energy difference is 0.03 kcal/mol).[34]

Equilibrium geometries, energies, and vibrational frequencies computed in this study are listed in Table 1, together with the corresponding experimental values.[32,33,35−46] According to the previous discussion, the structural parameters of MeONO shown in Table 1 refer to the trans conformation. More specifically, the theoretical parameters refer to the most stable trans conformer, the one with the energetically preferred methyl group orientation, as calculated by the CASSCF, MP2, and QCISD methods. The MP2 method predicts that the trans-eclipsed arrangement (a C−H bond eclipses the O−N bond) is the most stable trans conformation, contrary to that predicted by the CASSCF and QCISD methods. Nevertheless, the energy differences are almost negligible; that is, the calculations predict an almost free rotation for the methyl group,[34] which agrees with the fact that the precise orientation of the methyl group in this conformation has still not been experimentally determined.

In general, the agreement between the parameters calculated

(29) Gwinn, W. D.; Anderson, R. J.; Stelman, D. *Bull. Am. Phys. Soc.* **1968**, *13*, 831.
(30) Ghosh, P. N.; Bauder, A.; Günthard, Hs. H. *Chem. Phys.* **1980**, *53*, 39.
(31) Felder, P.; Ha, T.-K.; Dwivedi, V.; Günthard, Hs. H. *Spectrochim. Acta* **1981**, *37A*, 337.
(32) van der Veken, B. J.; Maas, R.; Guirgis, G. A.; Stidham, H. D.; Sheehan, T. G.; Durig, J. R. *J. Phys. Chem.* **1990**, *94*, 4029.
(33) Conboy, C. B.; Chauvel, J. P., Jr.; Moreno, P. O.; True, N. S.; Ott, C. M. *J. Phys. Chem.* **1986**, *90*, 4353.
(34) Martínez-Núñez, E.; Vázquez, S. A. *J. Chem. Phys.* **1997**, *107*, 5393.
(35) Turner, P. H.; Corkill, M. J.; Cox, P. *J. Phys. Chem.* **1979**, *83*, 1473.
(36) Bodenbinder, M.; Ulic, S. E.; Willner, H. *J. Phys. Chem.* **1994**, *98*, 6441.
(37) Dalby, F. W. *Can. J. Phys.* **1958**, *36*, 1336.
(38) Bowens, R. J., Hammerschmidt, J. A.; Grzeskowiak, M. M.; Stegink, T. A.; Yorba, P. M.; Polik, W. F. *J. Chem. Phys.* **1996**, *104*, 460.
(39) Duncan, J. L.; Mallinson, P. D. *Chem. Phys. Lett.* **1973**, *23*, 597.
(40) Stull, D. R.; Westrum, E. F., Jr.; Sinke, G. C. *The Chemical Thermodynamics of Organic Compounds*; Wiley: New York, 1969.
(41) Takagi, K.; Oka, T. *J. Phys. Soc. Jpn.* **1963**, *18*, 1174.
(42) Kuo, S.-C.; Zhang, Z.; Ross, S. K.; Klemm, R. B.; Jhonson, R. D., III; Monks, P. S.; Thorn, R. P., Jr.; Stief, L. J. *J. Phys. Chem. A* **1997**, *101*, 4035.
(43) Colwell, S. W.; Amos, R. D.; Handy N. C. *Chem. Phys. Lett.* **1984**, *109*, 525.
(44) Huber, K. P.; Herzberg, G. *Molecular spectra and molecular structure IV. Constants of diatomic molecules*; Van Nostrand: New York, 1979; Vol. 4.

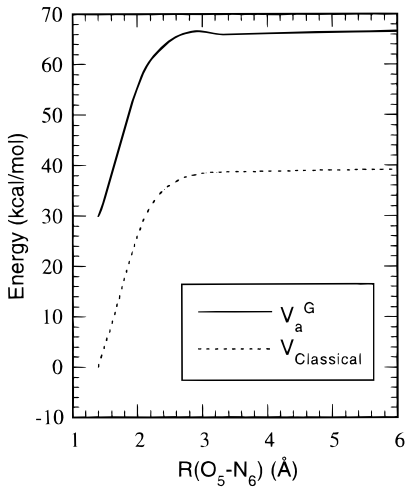

Figure 2. Classical potential ($V_{Classical}$) and vibrational adiabatic ground-state potential ($V_a^G(s)$) of the dissociation pathway as a function of the O−N distance.

by the different theoretical methods and the experimental data is good. As far as geometries are concerned, the most notable deviations are found between the MP2 and the QCISD values predicted for the four-center elimination state (see Figure 1 and Table 1). In particular, we remark the deviations found between structural parameters involving the hydrogen atom that is transferred in the elimination process (H_1).

MP2 and CASSCF frequencies were computed for the chemical species involved in the elimination and dissociation pathways, respectively. In general, the MP2 frequencies appear to be higher than the experimental ones for both the reactant and the elimination products. The CASSCF frequencies, however, do not follow a general trend when they are compared with the experimental data: they are higher for the reactant but lower for the dissociation products. Note that the agreement between experiment and theory (specially MP2) is good for the lowest frequencies, which have the most influence on the calculation of rate constants. The MP2 frequencies along the dissociation reaction path cannot, however, be employed for the dynamics calculations because the MP2 method does not describe appropriately the MeO−NO scission process.

The energy of the elimination transition state, relative to the *trans*-MeONO value, is calculated to be 40.94 kcal/mol at the MP2 level and 43.64 kcal/mol at the QCISD(T)//QCISD. As indicated in the foregoing section, we used the latter outcome to scale the MP2 MEP. The above values are in the order of that calculated by McKee[47] at the MP2/6-31G*//HF/6-31G* level (46.47 kcal/mol). The total relative energies computed here for the elimination products, 15.14 by MP2 and 14.38 by QCISD(T)//QCISD, are close to the experimental figure, 15.3 kcal/mol. For the products of dissociation, the theoretical value obtained at the QCISD(T)//CASSCF level, 39.29 kcal/mol, is somewhat lower than the recommended value for $D°_{298}$, 41.8 ± 0.9 kcal/mol,[45] based on Batt's data.[6]

3.2. Reaction Paths. The classical potential along the dynamically optimized DCP and its associated vibrationally adiabatic ground-state potential (V_a^G) obtained in this study for the N−O bond cleavage are depicted in Figure 2. As can be seen, the classical potential appears as a typical dissociation curve with a dissociation energy of 39.29 kcal/mol and no maximum ("loose" transition state). When the zero point energy contributions are added to construct the adiabatic potential, however, a maximum appears. Furthermore, the maximum in the GTS free energy of activation, which is the location of the CVT transition state, varies with the temperature as shown in Table 2: it shifts toward shorter O−N distances as the temperature increases. In the next section, we shall explain this behavior in terms of a generalization of the quasiequilibrium formulation of conventional TST.

Table 2. Position of the Maximum in the GTS for the Dissociation and Elimination Channels

	dissociation		elimination	
T/K	$R(O_5-N_6)$/Å	$V_a^G(s_*^{CVT})^a$	s_*^{CVT}/a_0	$V_a^G(s_*^{CVT})^a$
300	2.9341	66.53	−0.0038	69.55
400	2.9324	66.53	−0.0063	69.54
448.4	2.9316	66.53	−0.0068	69.54
457.7	2.9316	66.53	−0.0069	69.54
468.8	2.9308	66.53	−0.0070	69.54
473.0	2.9308	66.53	−0.0071	69.54
473.5	2.9308	66.53	−0.0071	69.54
500	2.9308	66.53	−0.0074	69.54
1000	2.7816	66.30	−0.0128	69.52
1500	2.2298	61.14	−0.0183	69.48

[a] Values in kilocalories per mole.

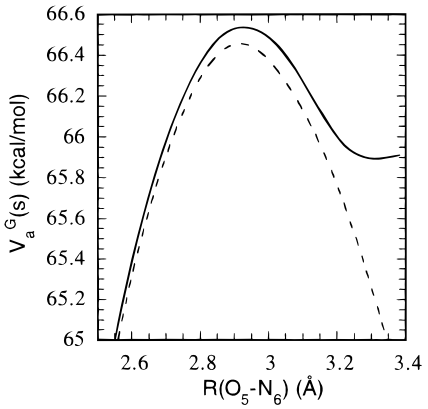

Figure 3. Vibrational adiabatic ground-state potential ($V_a^G(s)$) as a function of the O−N distance in the vicinity of the GTS, as calculated from the DCP (dashed line) and the DODCP (solid line).

To explore whether the DODCP presents significant alterations with respect to the DCP that could give rise to different kinetic predictions, we plotted in Figure 3 the adiabatic potential in the vicinity of the transition state as calculated from each classical path. At first sight, the two factors of the adiabatic potential governing the calculation of rate constants by CVT, the position of the maximum and the barrier height, for the two curves seem very similar. Nevertheless, the differences are large enough as to affect significantly the calculation of rate constants, as will be shown later.

The MEP and the adiabatic potential curve for the elimination process are plotted in Figure 4. The barrier height of the MEP for the forward reaction, the concerted elimination to form CH_2O and NO, is 43.64 kcal/mol. The position of the maximum moves toward the reactant as the temperature increases, which is the same trend as that found for the dissociation channel (see Table 2). For example, at 300 K, the maximum of the vibrationally adiabatic ground-state potential, V_a^G, is located at $s = -0.0038\ a_0$, and at 1500 K, the position is at $s = -0.0183\ a_0$.

Figure 5 shows the variation of several geometrical parameters along the elimination MEP. The MEP initially exhibits

(45) *Handbook of Chemistry and Physics*; Lide, D. R., Ed.; CRC Press: Boca Raton, FL, 1995−1996; Vol. 76.
(46) Endo, Y.; Saito, S.; Hirota, E. *J. Chem. Phys.* **1984**, *81*, 122.
(47) McKee, M. L. *J. Am. Chem. Soc.* **1986**, *108*, 5784.

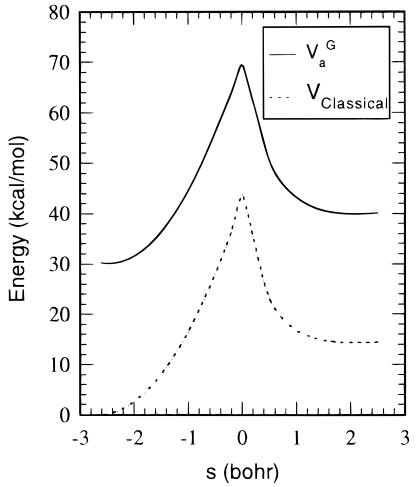

Figure 4. Minimum energy path ($V_{Classical}$) and vibrational adiabatic ground-state potential ($V_a^G(s)$) of the elimination channel.

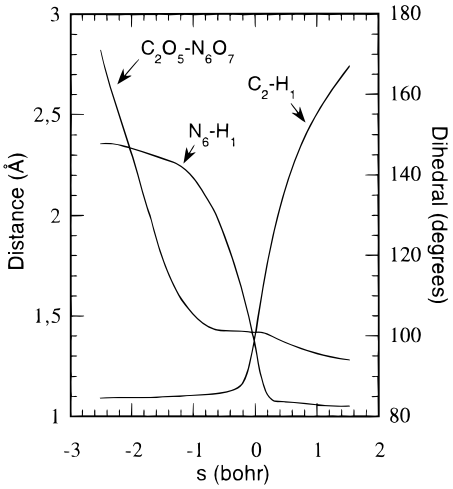

Figure 5. Variation of selected geometrical features along the elimination MEP.

a decreasing CO−NO dihedral angle, which changes markedly from 180° (reactant) to 100° (at $s \approx -0.8\ a_0$). The N−H_1 distance decreases significantly from $s \approx -1.0\ a_0$ to $s \approx 0.2\ a_0$, when the N−H bond is formed. Finally, the C−H_1 distance exhibits also a notable change from $s \approx -0.2\ a_0$, that is, very close to the transition state where the C−H bond is being broken.

Many vibrational frequencies experience significant changes in going from the reactant to the elimination products, especially close to the transition state (see Figure 6). For example, frequency 2823 cm^{-1}, which corresponds to a C−H stretch in the reactant region, changes markedly in the vicinity of the transition state and then it is transformed into the HNO bend in the product region. Similarly, frequency 1424 cm^{-1}, associated to a methyl bend, is transformed into the N−H stretch of the HNO compound in the product region; this change occurs basically in the interval between $s \approx 0\ a_0$ and $s \approx 0.2\ a_0$. Finally, vibrational frequencies associated to interactions that are not present in the products vanish when these species are formed. These interactions are the O−N stretch, the CON and ONO bends, and the methyl and CO−NO torsions.

3.3. Dynamical Study. 3.3.1. Dissociation. In this study, the dissociation pathway was investigated in the range of temperatures 300−1500 K. For this reaction channel, the dissociation path presents a "loose" transition state, which prevents one from using conventional TST. We applied CVT

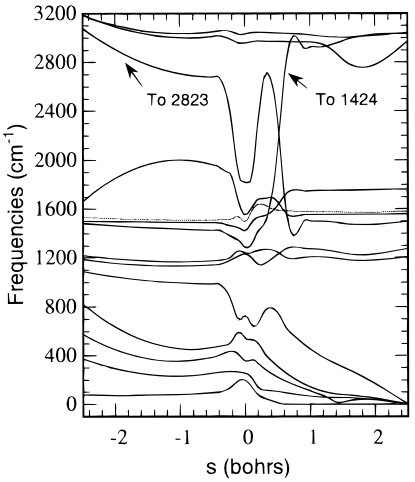

Figure 6. Variation of generalized vibrational frequencies along the elimination MEP.

to calculate dissociation rate constants using either the DCP or the dynamically optimized DCP. We also computed CAG transmission coefficients employing the DODCP to improve the rate constants. The rate constants are displayed in Table 3 and graphically in Figure 7. For the sake of comparison, we included high-pressure experimental rate constants extrapolated from rates obtained at 710 Torr and temperatures in the range 450−520 K.[8] Additionally, Table 4 gives the ratio between rate constants calculated by the different approaches, and Table 5 compares our calculated Arrhenius parameters with those determined experimentally.[8] It is found that our rate constants are somewhat higher than the experimental ones, except those estimated at 1500 K. The calculations performed with the DODCP afforded rate constants that are closer to the experimental values than are those obtained with the DCP. Furthermore, the theoretical figures are improved when the CAG transmission coefficients are included in the computations. This is also true for the Arrhenius parameters: the values calculated when the CAG factor was included are almost within the experimental uncertainties. Note that the CAG transmission factor computed at 1500 K is 0.15, a value extremely low; this might imply an inaccurate treatment of the thresholds.[25]

As indicated in the above section, the position of the maximum in the dissociation channel moves toward shorter O−N distances as the temperature increases (see Table 2). This behavior can be understood from the interpretation of the CVT rate constant that arises from generalizing the quasiequilibrium (or quasithermodynamic) formulation of conventional TST.[23] In this approach, the GTS rate constant is given by

$$k^{GT}(T,s) = \frac{\sigma k_B T}{h} K^0 \exp[-\Delta G^{GT,0}(T,s)/RT] \qquad (7)$$

where K^0 is the value of the reaction quotient evaluated at the standard state and $\Delta G^{GT,0}(T,s)$ is the generalized free energy of activation curve. This equation indicates that the minimum in $k^{GT}(T,s)$ corresponds to a maximum in $\Delta G^{GT,0}(T,s)$. There are two influences on the magnitude of $\Delta G^{GT,0}(T,s)$: the enthalpy change $\Delta H^{GT,0}(T,s)$ and the entropy change $\Delta S^{GT,0}(T,s)$:

$$\Delta G^{GT,0}(T,s) = \Delta H^{GT,0}(T,s) - T\Delta S^{GT,0}(T,s) \qquad (8)$$

The generalized free energy and its enthalpic and entropic contributions at 300 K as a function of the O−N distance are plotted in Figure 8. The generalized enthalpy was calculated in this study from the well-known Gibbs−Helmholtz equation,

Table 3. Theoretical and Experimental Rate Constants[a] for the Dissociation (k_I) and Elimination (k_{II}) Channels

	k_I/s^{-1}				k_{II}/s^{-1}				
T/K	CVT[b]	CVT[c]	CVT/CAG[c]	exptl[d]	TST	CVT	CVT/ZCT	CVT/SCT	exptl[e]
300.0	8.50(−12)	6.35(−12)	4.74(−12)	2.22(−13)	2.76(−16)	2.72(−16)	2.32(−15)	8.66(−15)	
400.0	3.74(−5)	2.88(−5)	2.32(−5)	3.25(−6)	4.77(−9)	4.69(−9)	1.44(−8)	2.86(−8)	
448.4	5.44(−3)	4.24(−3)	3.49(−3)	6.81(−4)	1.07(−6)	1.05(−6)	2.53(−6)	4.31(−6)	6.61(−6)
457.7	1.26(−2)	9.81(−3)	8.10(−3)	1.17(−3)	2.67(−6)	2.62(−6)	6.05(−6)	1.01(−5)	1.63(−5)
468.8	3.27(−2)	2.56(−2)	2.12(−2)	4.65(−3)	7.54(−6)	7.41(−6)	1.64(−5)	2.66(−5)	4.14(−5)
473.0	4.65(−2)	3.64(−2)	3.02(−2)	6.76(−3)	1.10(−5)	1.08(−5)	2.37(−5)	3.80(−5)	6.54(−5)
473.5	4.84(−2)	3.79(−2)	3.15(−2)	7.07(−3)	1.15(−5)	1.13(−5)	2.47(−5)	3.96(−5)	6.96(−5)
500.0	3.85(−1)	3.02(−1)	2.54(−1)	6.49(−2)	1.10(−4)	1.08(−4)	2.16(−4)	3.28(−4)	
1000.0	6.56(+7)	5.61(+7)	4.64(+7)	2.58(+7)	7.24(+4)	7.03(+4)	8.15(+4)	8.99(+4)	
1500.0	1.27(+10)	1.15(+10)	1.77(+9)	1.89(+10)	7.19(+7)	6.91(+7)	7.19(+7)	7.51(+7)	

[a] Powers of 10 in parentheses. [b] Calculations using the DCP. [c] Calculations using the DODCP. [d] Taken from ref 8. [e] Taken from ref 6.

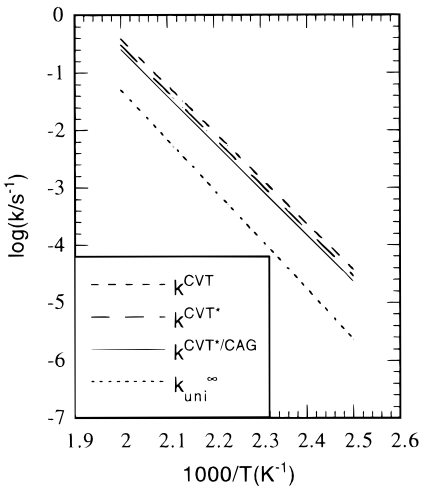

Figure 7. Arrhenius plot of experimental (k_{uni}^{∞}) and calculated rate constants for the dissociation channel. Calculations using the DODCP are indicated by the star symbol.

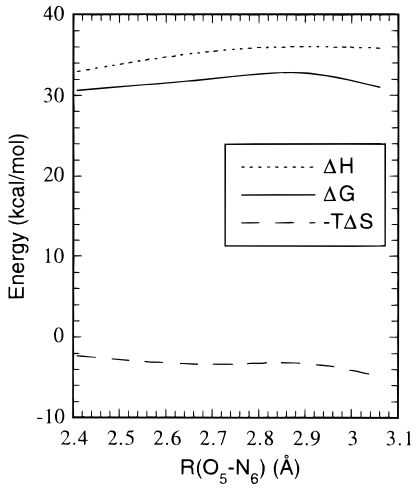

Figure 8. Gibbs energy profile and its enthalpic and entropic contributions at $T = 300$ K as a function of the O−N distance (dissociation process). All of the values are taken versus reactant.

Table 4. Ratios between Rate Constants Calculated by Various Methods for the Two Channels and Tunneling Transmission Factors for the Elimination Process

	dissociation[a]		elimination		
T/K	$k^{CVT}/k^{CVT\,b}$	$k^{CVT/CAG}/k^{CVT}$	k^{CVT}/k^{TST}	κ^{ZCT}	κ^{SCT}
300	0.75	0.75	0.98	8.58	31.99
400	0.77	0.80	0.98	3.10	6.15
448.4	0.78	0.82	0.98	2.42	4.12
457.7	0.78	0.83	0.98	2.33	3.88
468.8	0.78	0.83	0.98	2.23	3.62
473.0	0.78	0.83	0.98	2.20	3.54
473.5	0.78	0.83	0.98	2.20	3.53
500	0.79	0.84	0.98	2.02	3.07
1000	0.87	0.83	0.97	1.18	1.31
1500	0.91	0.15	0.96	1.04	1.09

[a] Calculations otherwise indicated were performed by using the DODCP. [b] Calculations using the DCP.

Table 5. Arrhenius Parameters: Activation Energies (E_a, in kcal/mol) and Pre-exponential Factors as $\log(A/s^{-1})$

	dissociation			elimination				
	CVT	CVT/CAG	exptl[a]	TST	CVT	CVT/ZCT	CVT/SCT	exptl[b]
$\log(A/s^{-1})$	17.47	16.53	16.01 ± 0.30	13.50	13.49	13.07	12.82	13.6 ± 0.6
E_a	40.60	38.88	39.6 ± 0.4	39.81	39.80	38.17	37.18	38.5 ± 1.0

[a] Taken from ref 8. [b] Taken from ref 6.

using a two-point central difference method. Then, eq 8 was employed to estimate the entropic contribution. As can be seen, $\Delta H^{GT,0}(T,s)$ increases as the separation between the fragments in the GTS increases, favoring a maximum in $\Delta G^{GT,0}(T,s)$ at large separations of the fragments in the GTS. $\Delta S^{GT,0}(T,s)$ is also maximized at large separations of the fragments because the freely rotating products correspond to a maximum in entropy. Therefore, the second term on the right-hand of eq 8 (a negative quantity) favors a maximum in $\Delta G^{GT,0}(T,s)$ at shorter separations of the fragments in the GTS, and this contribution becomes more and more important as T increases. As a result, the position of the maximum in the GTS shifts toward smaller O−N distances with increasing temperature (see Table 2).

3.3.2. Elimination. Variational transition-state theory rate constants for the elimination reaction computed in the temperature range 300−1500 K are tabulated in Table 3 and depicted graphically in Figure 9. Note that the symmetry number (σ) for this reaction is 2 because the saddle point has two enantiomers (C_1 symmetry). The ZCT and SCT transmission coefficients calculated at several temperatures are given in Table 4, together with the ratio between the rates computed by CVT and those obtained by conventional TST. Overall, the variational effects are found to be almost negligible, even at high temperatures. On the other hand, quantal effects, especially tunneling, may be significant because this decomposition channel involves the transfer of a light particle. The transmission factors obtained by the ZCT and SCT approaches show that in fact tunneling is especially important at low temperatures; particularly, at 300 K, $\kappa^{ZCT} = 8.58$ and $\kappa^{SCT} = 31.99$. At this temperature, the SCT transmission coefficient is about 4 times greater than the ZCT coefficient, indicating that inclusion of the curvature along the reaction path is important for a reliable representation of tunneling.

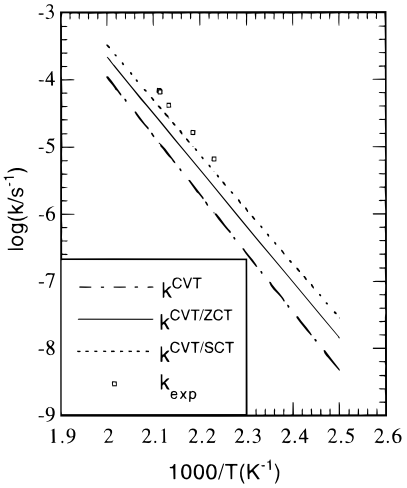

Figure 9. Arrhenius plot of experimental and calculated rate constants for the elimination channel. The squares are experimental data[6] obtained at temperatures in the range 443−473 K. The lines show the results obtained by CVT, including several approaches to take tunneling into account (see text).

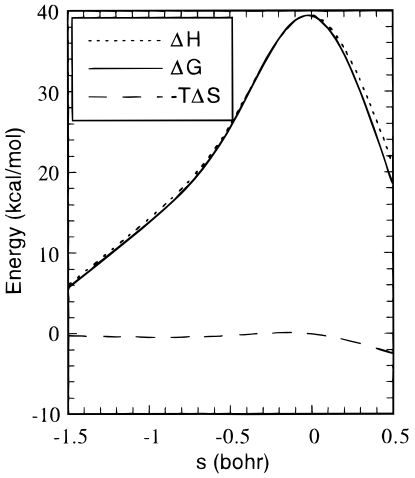

Figure 10. Gibbs energy profile and its enthalpic and entropic contributions at $T = 300$ K along the elimination MEP. All the values are taken versus reactant.

For the sake of comparison, Table 3 includes the rate constants achieved experimentally at temperatures in the range 443−473 K.[6] The theoretical and experimental rate constants for this reaction channel are much smaller than those obtained for the dissociation process. This could be expected considering that the barrier height for the elimination channel is higher than that for the dissociation. Nevertheless, this is not the only factor that makes the rates of these two channels so different, as will be shown below. We found that the rates are improved when tunneling is included in the computations. Specifically, the CVT/SCT calculations afforded rate constants that conform very well with the experimental ones. Good agreement is also evident when our Arrhenius parameters are compared with those determined experimentally: in most cases, the theoretical parameters are within the experimental errors (see Table 5).

As indicated above, the position of the GTS for the elimination process, as well as for the dissociation, shifts toward the reactant with increasing temperature. The explanation given before to clarify the trend found in the dissociation process is, however, not appropriate here because the elimination reaction path presents a tight transition state. This makes $\Delta H^{GT,0}$ decrease notably as the reaction coordinate increases from zero, on the contrary to the behavior presented in the dissociation process. Furthermore, the variation of $\Delta S^{GT,0}$ with the reaction coordinate is also significantly different here. In fact, from eq 8 and the Gibbs−Helmholtz equation we estimated that $\Delta S^{GT,0}$ is almost insignificant for the elimination channel. For the sake of example, we show graphically in Figure 10 how these thermodynamic quantities evaluated at 300 K vary along the reaction path. From this analysis, we conclude that the O−N bond cleavage is considerably faster than the elimination process not only because the barrier height for the O−N bond cleavage is lower than that for the elimination reaction but also because the former process is entropically favored.

4. Concluding Remarks

Direct dynamics calculations were performed to explore the two competing channels that initiate the thermal decomposition of methyl nitrite. Electronic structure data were obtained by using the standard 6-311++G(d,p) basis set and the CASSCF, MP2, and QCISD methods. Canonical variational transition-state theory was applied to compute thermal rate constants for the dissociation and elimination processes, at temperatures in the range 300−1500 K.

A DCP for the dissociation process was constructed, taking the O−N distance as the distinguished coordinate. The dissociation energy was computed to be 39.29 kcal/mol by QCISD(T)/6-311++G(d,p)//CASSCF(8,8)/6-311++G(d,p) calculations. Subsequently, the DCP was improved by an algorithm[21] in which the orientation of the dividing surface is optimized (DODCP). For the elimination pathway, our calculations led us to predict a four-center transition state and a MEP that connects this transition state with the trans conformation of MeONO. The elimination barrier height was calculated as 43.64 kcal/mol at the QCISD(T)/6-311++G(d,p)//QCISD/6-311++G(d,p) level of theory.

The rate constants evaluated for the O−N bond scission, the main unimolecular decomposition channel, are rather higher than the experimental ones.[8] Our best results are those achieved by the DODCP and including the CAG transmission coefficients in the calculations. For these calculations, the Arrhenius parameters are practically within the experimental errors.

For the elimination process, the results were improved when tunneling was taken into account. In particular, the CVT/SCT calculations predicted rate constants that are in good agreement with those determined experimentally,[6] indicating that tunneling in the elimination process is reliably represented by the SCT approach. On the other hand, the rate of the elimination reaction is quantitatively insignificant compared with the rate of the dissociation process. This is a result of two factors that take part in the same direction. First, the barrier height for the O−N bond scission is lower than that for the elimination channel, and second, the dissociation process is entropically favored.

The results presented in this study are encouraging for the ability of direct dynamics calculations to be able to predict reliable rate constants for rather complex chemical reactions in the gas phase.

Acknowledgment. The authors are very grateful to Dr. D. G. Truhlar for his generous provision of the POLYRATE 7.8.1 package program. We thank J. Villà for helpful discussions. A.F.-R. and E.M.-N. also thank Xunta de Galicia for a grant.

JA9809307